CFA/VISHNO 2016

# Transitoire et changement de régime des écoulements redressés de Rayleigh à forts niveaux : Etudes numérique et expérimentale

V. Daru[a], H. Bailliet[b], D. Baltean Carlès[c], I. Reyt[a] et C. Weisman[c]
[a]DynFluid Lab., ENSAM, LIMSI-CNRS, 151 bd de l'hôpital, 75013 Paris, France
[b]Institut PPRIME,UPR CNRS 3346,Université de Poitiers,ISAE-ENSMA, 6 rue Marcel Doré, 86073 Poitiers, France
[c]Université Pierre et Marie Curie, LIMSI-CNRS, 4 Place Jussieu, 75252 Paris, France
helene.bailliet@univ-poitiers.fr

Acoustic streaming is a second order flow associated with an acoustic wave and generated by the interaction between the wave and a solid wall. In the case of a stationary plane wave at low amplitude i.e. for slow streaming flow, the behaviour of this second order flow is well known: the streaming velocity along the resonator axis is a quadratic function of the acoustic velocity amplitude. For higher acoustic levels i.e. fast streaming flow, a previous numerical study (Inertial effects on non linear acoustic streaming, V. Daru, D. Baltean Carlès, C. Weisman, AIP Conf. Proc. 1685, 030003 (2015)) has shown that this streaming velocity becomes a linear function of the acoustic velocity amplitude. In this new flow regime, additional streaming cells has been observed inside the resonator. In the present work, experimental results are presented that confirm the numerical observations. LDV measurements are conducted on a system of different physical dimensions from but similar asymptotic scales as the numerical study. The order of magnitude of streaming velocities on the resonator axis and in the near-wall region are compared for both flow regimes. Transient evolution of streaming velocity for various locations are also analysed for both flow regimes in order to point out the associated characteristic time scales.

# 1 Introduction

Rayleigh streaming refers to the second order mean flow that is generated by effects related to the interaction between a solid surface and an acoustic wave [1]. In thermoacoustic devices, acoustic streaming results in convected heat flow that can reduce the efficiency. Since the power density of a thermoacoustic device depends on the acoustic amplitude, high acoustic amplitude phenomena need to be controled. A better understanding of the corresponding so-called "fast" Rayleigh streaming is therefore useful to assess its impact on the efficiency of thermoacoustic devices. For fast streaming flow, a previous numerical study [2] has shown that this streaming velocity changes from a quadratic to a linear function of the acoustic velocity amplitude.

In the present study, numerical and experimental results are gathered in order to describe a change of regime at high acoustic amplitudes, characterised by the change of dependence between the streaming velocity and the acoustic amplitude going from a quadratic dependence ($U_s = O(U_{ac}^2)$) to a linear dependence ($U_s = O(U_{ac})$). Section II presents the numerical method and the experimental setup and procedure. In Section III, the results are presented describing the characteristics of the two streaming flow regimes. Moreover, the time evolution of streaming velocity is presented as a first step for understanding the evolution of the streaming pattern.

# 2 Experimental and numerical methods

## 2.1 Problem description and numerical method

We consider a cylindrical tube of length $L$ and radius $R$, initially filled with air at pressure $p_0$ and density $\rho_0$ equal to $101325Pa$ and $1.2kg/m^3$. The viscosity of air is supposed to be constant, $\mu = 1.795\ 10^{-5}kgm^{-1}s^{-1}$. The instantaneous flow is calculated with a Direct Numerical Simulation approach and the mean flow is obtained by time averaging over an acoustic period. An acoustic standing wave is initiated by shaking the tube in the axial direction with given amplitude and frequency. The flow is modeled by the compressible Navier-Stokes equations expressed in the moving frame attached to the tube, so that a forcing source term is added. In the oscillating flow that we consider, shock waves can develop (as shown in [3]), but they are of small intensity, it was also shown that the wave propagation can be considered as isentropic. We thus simplify the fully compressible model by considering an isentropic state law for air, given by $p - p_0 = c_0^2(\rho - \rho_0)$, where $p$, $\rho$ and $c_0$ are respectively the pressure, density and sound velocity. Therefore the energy equation is decoupled from the other equations and we only solve the mass and momentum equations, excluding thermal effects in our study.

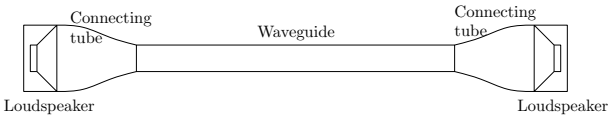


FIGURE 1 – Diagram of the experimental apparatus.

The physical boundary conditions in the moving frame are: no slip on the boundary walls parallel to horizontal symmetry axis, and symmetry conditions on the vertical boundaries. Resonant conditions are imposed, for which $L = \lambda/2$, $\lambda = c_0/f$ being the wave length, and $f$ the fundamental vibration frequency of the resonator. The equations are numerically solved with an axisymmetric formulation using high order finite difference schemes [3, 4]. The mean flow is obtained from calculating a simple mean value for each physical quantity (velocity, pressure, density) over an acoustic period.

All results presented below are obtained using a regular mesh of rectangular cells composed of 500 points in the axial direction, and of $5 \times R/\delta_\nu$ points in the radial direction, with $\delta_\nu = \sqrt{2\nu/\omega}$ the acoustic boundary layer thickness, $\omega$ being the pulsation. The time step $\delta t$ is fixed in order to insure stability of the numerical scheme.

## 2.2 Experimental setup

The setup used to observe the phenomenon of acoustic streaming is shown in Fig. 1 and consists in a cylindrical tube connected at each end to a loudspeaker via connecting tubes designed to avoid separation effect related to the singularities in change of section. The cylindrical part of the waveguide has inner radius $R = 19.5$ mm and the waveguide is filled with atmospheric air. The total length of the wave guide is $L_{exp} = 2.13$ m and the system is tuned on one of the two distinct frequencies corresponding to two different resonant modes: either the first mode corresponding to $L_{exp} = \lambda/2$ or the third mode corresponding to $L_{exp} = 3\lambda/2$.

The acoustic wave is generated by two loudspeakers driven by a wave generator whose frequency and amplitude are controlled. Wood smoke is used as seeding particles in order to perform LDV measurements. The single component LDV system is a Dantec Dynamic Model 2580, the probe is mounted on a three-axis positioning system. The argon

krypton laser has an optical wavelength of 514.5$\mu m$ and a power of 25 W. The parameters of LDV system are adjusted for sound measurements and the axial streaming velocity is measured following the work of Valière *et al.* [5] along the centerline of the guide. In agreement with Moreau *et al.* [6], measurements are performed more than 26 min after the acoustic field is switched on and are stable after this time. Also, following this latter reference, in order to reach convergence in the measured streaming velocity, we choose to acquire either 70000 points or to stop acquisition after 10 seconds. This gives a good compromise between a sufficient number of measured tracer particles per point for a precise streaming velocity measurement and a small measuring time that insures a correct seeding during the whole measurement.

A set of measurements is also performed by PIV. A laser sheet of 1 mm thickness is generated by a pulsed laser (Quantel Mini-Yag) having a 532 nm wavelength, issuing a pulsed energy of 30 mJ and synchronized with a maximum frequency of 20 Hz. To insure convergence of the streaming velocity field calculation, 500 pairs of pictures were recorded by a JAI RM-4200CL camera (maximum of 15 pictures/second, 2048 × 2048 pixels) and the 500 calculated velocity fields are averaged. This installation allows the discretization of the velocity field with resolution along the guide axis/radius $\Delta x = \Delta r = 0.52$ mm. For more information on the evaluation of the streaming velocity see the work of Reyt *et al.* [7].

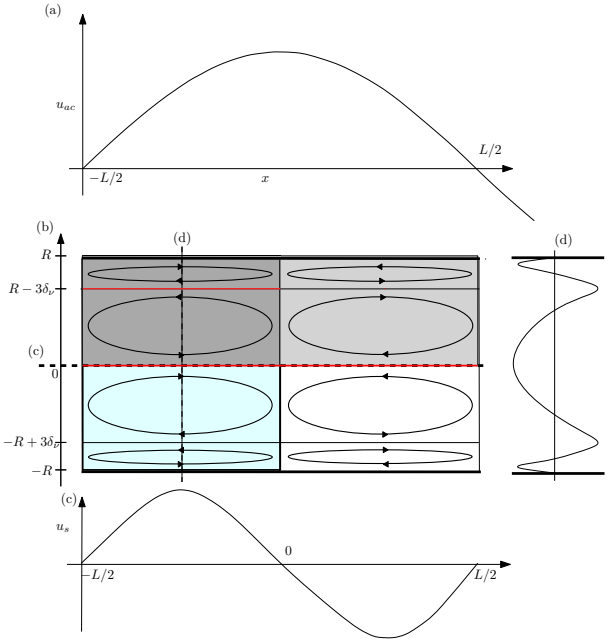


FIGURE 2 – (a) Acoustic wave pattern. (b) Schematic representation of the corresponding slow streaming velocity field. Grey and dark grey zone : simulation domain. Blue and dark grey zone : PIV measurement. Red lines : LDV measurement. (c) Variation of axial streaming velocity with respect to the axial coordinate at $r = 0$. (d) Variation of axial streaming velocity with respect to the radial coordinate at $x = \lambda/8$.

# 3 Results

The Rayleigh streaming pattern in a standing wave resonator is well known. A schematic representation is given in Fig. 2. The simulation domain is shown in grey. The profiles obtained by LDV correspond to the horizontal red lines (along the resonator axis and in the near wall region) and the PIV measurement domain is the light blue/dark grey zone. Streaming vortices are of toroidal shape with a $\lambda/2$ spatial periodicity. In the outer cells (located in the resonator core) the flow is circulating from the acoustic velocity nodes towards the acoustic velocity antinodes along the central axis and returns in the vicinity of the wall to complete a closed loop. At the location $r = R - 3\delta_\nu$ the streaming flow separates into two cells (inner cell and outer cell) and the amplitude of the axial streaming velocity has a local maximum (Fig. 2.d) called the inner streaming amplitude. In the inner cells (located in the near wall region) the flow rotates in the opposite direction. Note that in Fig.2.b, the represented guide is narrow (the ratio $R/\delta_\nu$ is about 4) in order to show the two types of cells. In the present study, $20 \leq R/\delta_\nu < 140$ and thus inner vortices fill a much smaller portion of the guide.

## 3.1 Studied configurations

In this study we compare results from two experimental (noted $E_1$ and $E_2$) and four numerical ($N_1$ to $N_4$) configurations. The corresponding parameters are summarised in Table 1. For all configurations the control variable is $U_{ac}$, the amplitude of the axial acoustic velocity. The range of variation of $U_{ac}$ shown in Tab. 1 is chosen to encompass a variety of streaming flows in order to exhibit the different flow regimes (between 6 and 19 values of $U_{ac}$ for each case). To that effect the relevant difference between the configurations is the value of the geometrical aspect ratios $R/\delta_\nu$ and $R/L$. The tuning frequency $f$ in the $E_1$ experiment is different from that of $E_2$ resulting in a change of $L$ and $\delta_\nu$ and consequently of $R/L$ and $R/\delta_\nu$ (Table 1). In the numerical simulations, the frequency $f$ and the tube radius $R$ can be varied independently (Table 1).

TABLE 1 – Parameters of the different presented cases.

| Name | $f(Hz)$ | $R/\delta_\nu$ | $R/L$ | $U_{ac}(m/s)$ | $U_s(m/s)$ |
|---|---|---|---|---|---|
| $N_1$ | 20000 | 20 | 0.09 | [0.2−60] | [$0.4e^{-4}$−2.4] |
| $N_2$ | 20000 | 40 | 0.09 | [0.4−80] | [$1.6e^{-4}$−4.9] |
| $N_3$ | 20000 | 50 | 0.09 | [0.5−73] | [$2.6e^{-4}$−4.2] |
| $N_4$ | 5000 | 50 | 0.045 | [0.5−62] | [$2.6e^{-4}$−3.3] |
| $E_1$ | 88 | 84 | 0.01 | [2.7−45] | [$90e^{-4}$ − 1.5] |
| $E_2$ | 240 | 138 | 0.027 | [2.7−30] | [$80e^{-4}$ − 0.4] |

## 3.2 Two flow regimes

In the Rayleigh streaming theory, for very large tubes, the axial streaming velocity amplitude $U_s$ is a quadratic function of the acoustic velocity amplitude $U_{ac}$ :

$$U_{s_{Rayleigh}} = \frac{3}{8}\frac{U_{ac}^2}{c_0} \quad . \tag{1}$$

Results found in the present study show that a dependence upon the aspect ratio $R/\delta_\nu$ should be included in eq. 1 for slow streaming that can be expressed by the

following relation :

$$U_s \propto \left( U_{ac} \left( \frac{R}{\delta_\nu} \right)^{0.15} \right)^2 \quad . \tag{2}$$

Figure 3 represents the variation of the axial streaming velocity amplitude $U_s$ against the product $U_{ac} \times \left(\frac{R}{\delta_\nu}\right)^{0.15}$ (on a linear scale in Figure 3.a and on a log-log scale in Figure 3.b). In Figure 3.b, the ordinate $U_s^*$ is defined as $U_s/U_{s_{Rayleigh}}$ scaled by its value at the lowest acoustic velocity so that at low regime all the curves start from 1. It confirms that at low regime the quadratic dependence is satisfied (all points fall on the horizontal line $U_s^* = 1$). The corresponding flow regime is thereafter called the first regime (Regime 1). Figure 3.a shows that in each configuration the quadratic dependence is only true up to a certain value of $U_{ac} \times \left(\frac{R}{\delta_\nu}\right)^{0.15}$. The dependence then becomes linear, with different slope for each numerical or experimental configurations (straight lines departing from the quadratic curve in Fig. 3.a). This is confirmed in Figure 3.b since all curves are of slope $-1$ on a log-log scale. The corresponding flow regime is thereafter called the second regime (Regime 2).

## 3.3 Evolution of the streaming pattern

It was found in previous experimental and numerical studies [7, 3] that fast acoustic streaming is characterised by the emergence of an additional streaming cell. We therefore searched for a correlation between the appearance of this cell and the change of regime described above.

Figures 4.a,b,c show isolines of the axial streaming velocity colored by its value and the streamlines of the streaming flow for one of the $N_3$ numerical simulations belonging to Regime 1 (Fig. 4.a) and Regime 2 (Fig. 4.b,c). The emergence (Fig. 4.c) of counter-rotating cell along the resonator axis ([3, 7]) can only be seen in Regime 2. Since there is no extra cell in Figure 4.b of Regime 2 there is no direct correlation between the transition to the second regime and the appearance of a new cell. Moreover there exist configurations in Regime 2 where the emergence of the extra cell has not been observed yet ($N_4$). This seems to be related to the fact that the aspect ratio $R/L$ is different between $N_3$ and $N_4$. Figure 4.d shows the isolines of the axial streaming velocity colored by its value obtained by PIV for an experimental data set ($E_2$) belonging to Regime 2. Note that the area of positive velocity (the yellow/red area) is supposed to be continuous (forming a half C-shape) but because of light reflections on the tube glass, the PIV datas are altered. Figures 4.b,c,d show how distorted the streaming flow in the core region becomes in Regime 2.

The change in the streaming pattern is less important in the near-wall region (Fig. 4). While $U_s$ decreases greatly in the core region in Regime 2 (see color map in Fig. 4.b,c,d), it does only slightly decrease in the near-wall region. The position of the streaming velocity maximum in the near-wall region only shifts toward the acoustic velocity node as the acoustic level increases.

Figure 5 shows the variation of the axial streaming velocity amplitude $U_s$ within the near-wall region against the product $U_{ac} \times \left(\frac{R}{\delta_\nu}\right)^{0.15}$ on a linear scale. The quadratic dependence is preserved for both regimes. In the simulation, the values of $U_{s\ near-wall}$ are taken at the axial position of streaming velocity maximum at $r = 3\delta_\nu$, corresponding

(a)

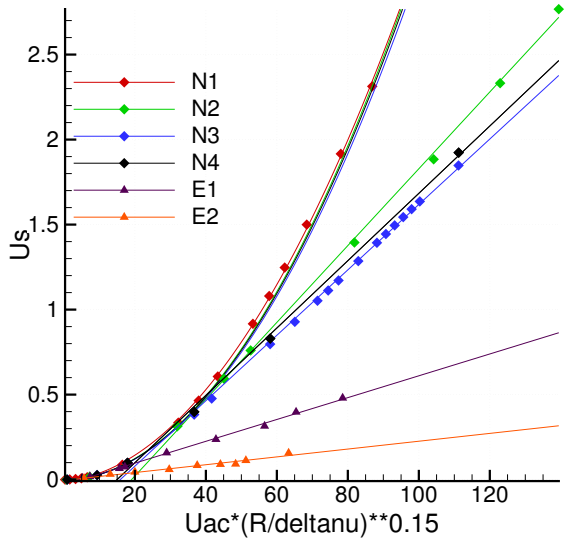


(b)

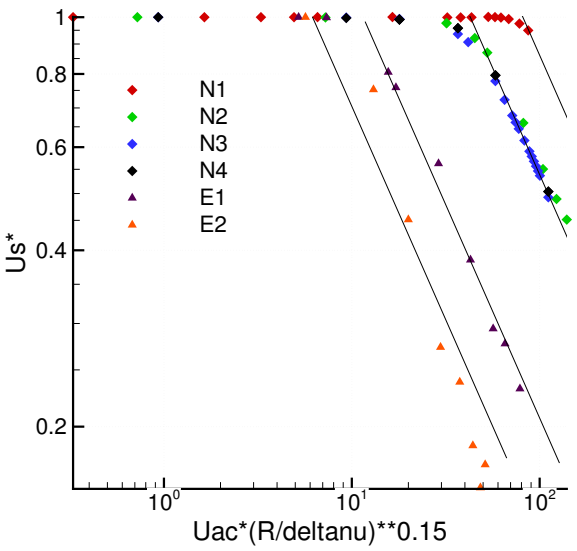


FIGURE 3 – $U_s$ against $U_{ac} \times \left(\frac{R}{\delta_\nu}\right)^{0.15}$, on a linear scale (a) and on a log-log scale (b).

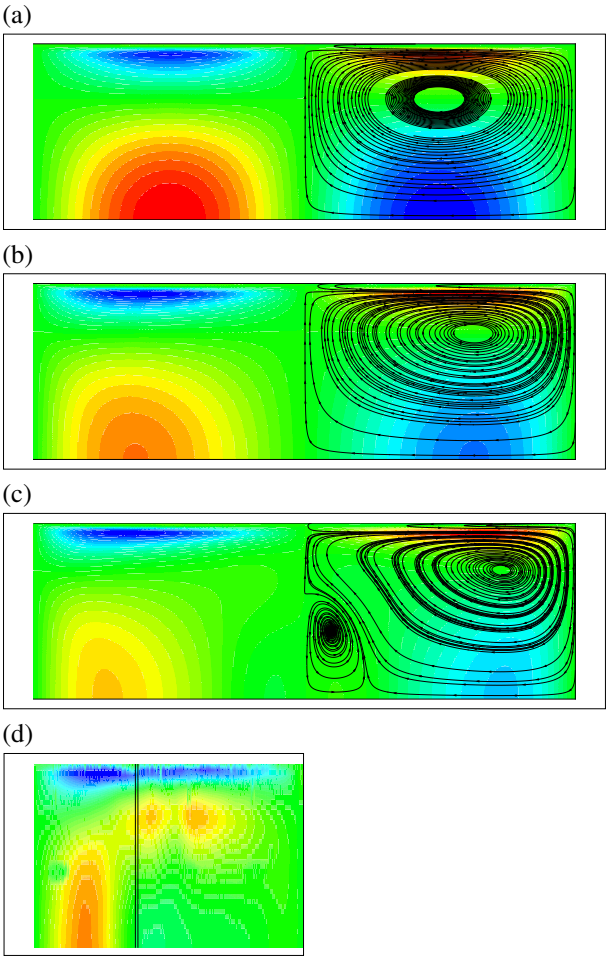


FIGURE 4 – Isolines of the axial streaming velocity colored by its value and the streamlines of the streaming flow. (a) $N_3$ Regime 1, (b) $N_3$ Regime 2, (c) $N_3$ Regime 2, (d) $E_2$ Regime 2.

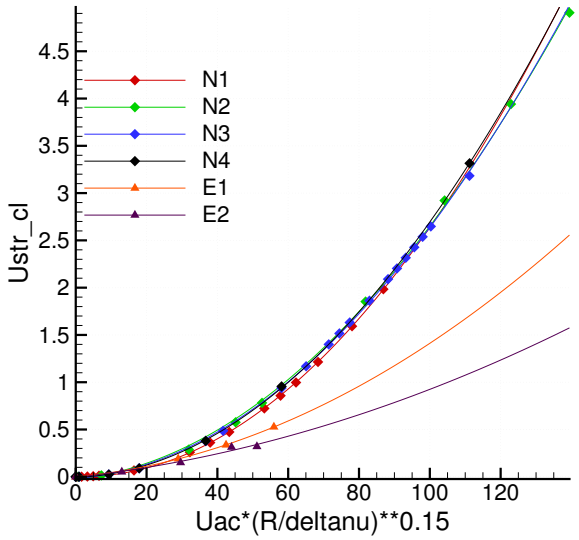


FIGURE 5 – $U_s$ against $U_{ac} \times \left(\frac{R}{\delta_\nu}\right)^{0.15}$ on a linear scale within the near-wall region.

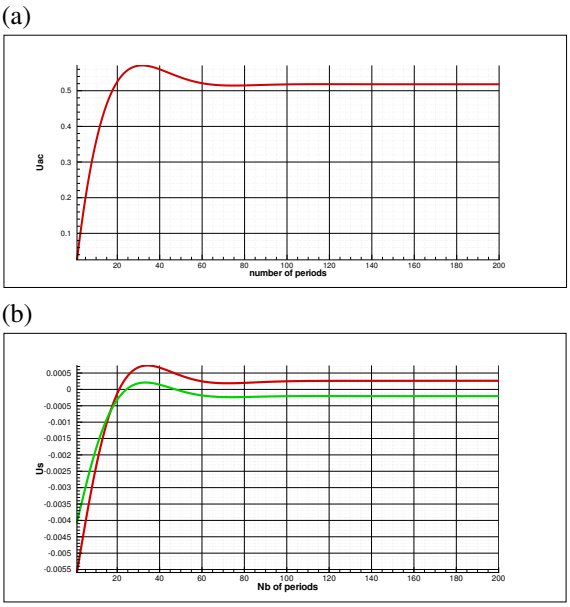


FIGURE 6 – Time evolution $N_3$ Regime 1. (a) (–) Acoustic velocity at $r = 0$, $x = 0$, (b) (–) Streaming velocity at $r = 0$, $x = -L/4$ and (–) Streaming velocity at $r = R - 3\delta_\nu$, $x = -L/4$.

to the inner streaming amplitude. All simulation points follow the same curve. Experimental datas are taken in the near-wall region but it could not be precisely set at the same relevent position. In $E_1$, the points are measured at $3\delta_\nu$ but not at the axial position of the streaming velocity maximum, whereas in $E_2$, they are measured at the axial position of streaming velocity maximum somewhere in the near wall region. The difference in the measurement position can explain the fact that the experimental datas do not follow the same curve, but quadratic curves of smaller streaming velocity levels. However, in each case the quadratic dependence is kept.

Finally, the change of regime appears to depend on different parameters including $R/\delta_\nu$ and $R/L$. An additional transition can be observed in Regime 2 with the appearance of an extra counter-rotating streaming cell in the core. Further analysis of this transition is currently under study [8].

## 3.4 Time evolution

Time evolution of the acoustic streaming velocity is studied at different locations in the streaming cell, inside the boundary layer and in the core of the waveguide. Here this evolution is assessed against the time establishment of the acoustic velocity.

At slow streaming (Regime 1), numerical time evolutions of the acoustic velocity and the velocity averaged over a period are represented in Figure 6 for the slowest flow regime of $N_3$. The location selected for the acoustic velocity is the waveguide center, $r = 0$ and $x = 0$ (Figure 6.a). Two locations are selected in the streaming pattern (Figure 6.b): the outer streaming cell center $r = 0$ and $x = -L/4$ (in red) and at the place of the inner streaming amplitude, $r = R - 3\delta_\nu$ and $x = -L/4$ (in green). The observed time evolutions are similar for all three curves. Once the acoustic field is established, the velocity averaged over a

period is indeed the streaming velocity, but until then it is physically meaningless. For these cases the establishment of streaming cannot be distinguished from that of the acoustic field. Experimentally it was shown that the establishment of streaming follows the acoustics in the slow streaming regime [7] in agreement with with results shown in Figure 6.

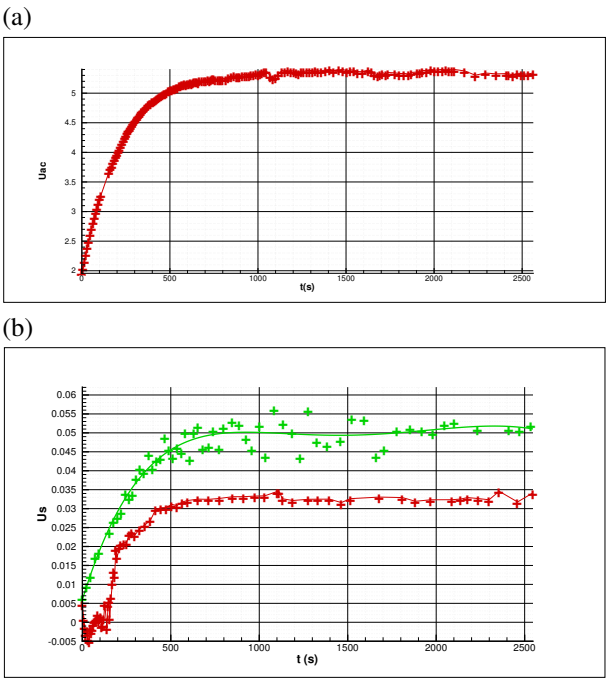


FIGURE 7 – Time evolution $E_2$, beginning of Regime 2. (a) (–) Acoustic velocity at $r = 0$, $x = 0$, (b) (–) Streaming velocity at $r = 0$, $x = -L/4$ and (–) Streaming velocity at $r = R - 3\delta_\nu$, $x = -L/4$.

Figure 7 shows time evolutions of the acoustic field and the streaming field for an experimental investigation of $E_2$ in the beginning of Regime 2 (before the appearance of the extra cell). The selected locations and the color codes are the same as in Figure 6. In the inner cell, the establishment of the streaming flow still follows the acoustics while in the core the time evolution of the streaming flow is starting to be distinct from that of the acoustic field. Note that the time scale of experimental and numerical evolutions are very different due to the difference in frequency.

Figures 8 and 9 (for $N_3$ and $E_2$ respectively) address cases in Regime 2 when the extra streaming cell is present in the established streaming flow. The onset of acoustics is shown in Figures 8.a and 9.a. Note that in Figure 8.a, the time evolution is shown for a small number of period translating the rapidity of the establishment of acoustics in this case. The numerical time evolutions of the velocity averaged over a period are plotted once the acoustics is established (Figure 8.b) in order to show the meaningfull establishment of the streaming flow. Time evolution of the streaming velocity at the place of inner streaming amplitude (noted $I$) is plotted in dark green in Figures 8.b and 9.b. The inner streaming still follows the acoustics.

In the resonator the focus is on three different locations: the geometrical center of the streaming cell ($r = 0$ and $x = -L/4$, noted $O_c$), the place of the established outer streaming cell maximum ($r = 0$ and $x$ corresponding to the maximum amplitude and brightest color in Figure 4.c,d, noted $O_m$) and the place of the established extra countra-

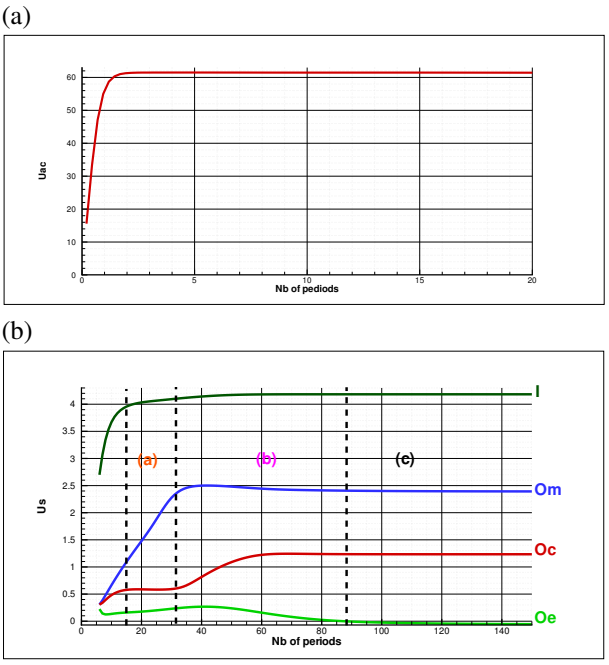


FIGURE 8 – Time evolution $N_3$ Regime 2 and extra cell (a) (–) Acoustic velocity at $r = 0$, $x = 0$, (b) (–) Streaming velocity at $I$, (–) Streaming velocity at $O_c$, (–) Streaming velocity at $O_m$ and (–) Streaming velocity at $O_e$.

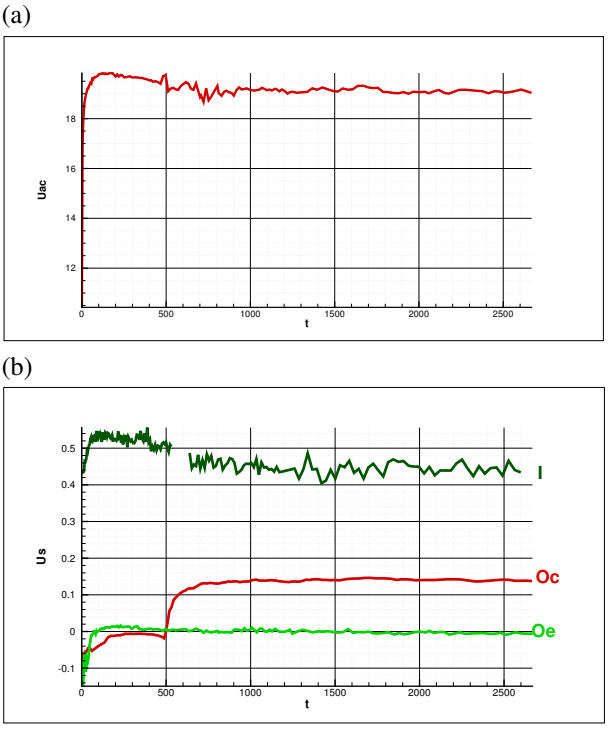


FIGURE 9 – Time evolution $E_2$ and extra cell. (a) (–) Acoustic velocity at $r = 0$, $x = 0$, (b) (–) Streaming velocity at $I$, (–) Streaming velocity at $O_c$, (–) Streaming velocity at $O_e$.

rotating streaming cell amplitude ($r = 0$ and $x$ corresponding to the center of the corresponding streamlines in Figure 4.c, noted $O_e$). Different qualitative behaviours are observed depending on the location. A careful look at the profiles in Figure 8.b brings out three different time intervals that are named (a), (b) and (c). Similar zones can be observed on the experimental measurements (Fig. 9.b). In order to

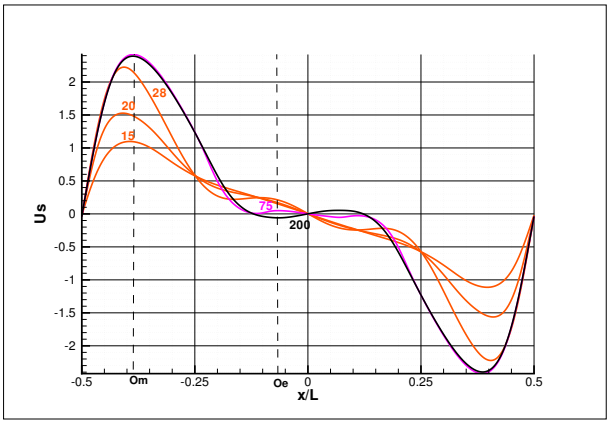


FIGURE 10 – Axial profiles of $U_s$ at $r = 0$ for selected times in zones (a), (b) and (c) (refer to Fig.8) numbered according to the period number.

get further insight into the streaming pattern evolution, Figure 10 shows several velocity profiles on the waveguide axis at selected times in the different zones (orange for zone (a), purple for zone (b) and black for zone (c)) numbered according to the period number. For the location $O_m$ (in blue in Figure 8.b and on the vertical dashed line labeled $O_m$ in Figure 10), the velocity increases during time interval (a) up to its maximum value. The actual position of the maximum of the outer streaming velocity shifts slightly with time towards $O_m$. For the location $O_c$ (in red in Figure 8.b and at $x/L = 0.25$ in Figure 10), the velocity remains constant during time interval (a): the red curve exhibits a plateau (Fig. 8.b) and the three orange curves intersect (Fig. 10). During the time interval (b), there is a spatial rearrangement of the outer streaming pattern (purple curve in Figure 10). For the location $O_e$ (in green in Figures 8.b and 9.b) both the experimental and numerical evolutions show that the velocity is positive before becoming negative meaning that the contra-rotating cell appears after a certain time. Note that the appearance of the extra cell does not modify the time evolution for the other locations in the streaming field (zone (c) on Figure 8.b).

Finally, the inner streaming establishment is correlated to that of acoustics regardless of the regime, whereas the outer streaming time evolution depends on the flow regime. In Regime 2, two different time scales were observed which we relate to velocity increase followed by a spatial rearrangement of the streaming flow.

# 4 Conclusion

A study including numerical and experimental results was presented in order to analyse the different streaming flow regimes in a cylindrical wave guide. Two different regimes were indentified. The first regime, Regime 1, corresponds to a slow streaming flow where the streaming velocity amplitude is a quadratic function of the acoustic amplitude. In the second regime, Regime 2, streaming velocity becomes a linear function of the acoustic amplitude. The change of regime depends on different parameters including $R/\delta_\nu$ and $R/L$. An additional transition can be observed in Regime 2 with the appearance of an extra counter-rotating streaming cell in the core. Further analysis of this transition is the object of future work. A compared numerical and experimental study of the time evolution of the streaming flow was also conducted for the different flow regimes. The inner streaming establishment is correlated to that of acoustics regardless of the regime. The outer streaming time evolution depends on the flow regime. In Regime 2, two different time scales were observed which we relate to velocity increase followed by a spatial rearrangement of the streaming flow.

# References

[1] L. Rayleigh, On the Circulation of Air Observed in Kundt's Tubes, and on Some Allied Acoustical Problems, *Philos. Trans. R. Soc.* **175**, 1-21 (1884)

[2] V. Daru, D. Baltean-Carlès, C. Weisman, Inertial effects on non linear acoustic streaming, *AIP Conf. Proc.* **1685**, 030003 (2015).

[3] I. Reyt, V. Daru, H. Bailliet, S. Moreau, J. C. Valière, D. Baltean-Carlès and C. Weisman, Fast acoustic streaming in standing waves: Generation of an additional outer streaming cell, *J. Acoust. Soc. Am.* **134**(3), 1791-1801 (2013).

[4] V. Daru, D. Baltean-Carlès, C. Weisman, P. Debesse and G. Gandikota, Two-dimensional numerical simulations of nonlinear acoustic streaming in standing waves, *Wave Motion* **50**, 955-963 (2013).

[5] J.-C. Valière, S. Moreau, H. Bailliet, Development of laser techniques for acoustic boundary layer measurements. PART I: LDV signal processing for high acoustic displacements, *Acta Acustica united with Acustica* **95** , 585-594 (2009).

[6] S. Moreau, H. Bailliet, J.-C. Valière, Measurements of inner and outer streaming vortices in a standing waveguide using laser doppler velocimetry, *J. Acoust. Soc. Am.* **123**, 640-647 (2008).

[7] I. Reyt, H. Bailliet, J. C. Valière, Experimental investigation of acoustic streaming in a cylindrical wave guide up to high streaming Reynolds numbers, *J. Acoust. Soc. Am.* **135**, 27-37 (2014).

[8] V. Daru, D. Baltean-Carlès, I. Reyt, C. Weisman, Streaming non linéaire : rôle de la composante radiale acoustique, *CFA Proc.* (2016).